

# Wasserstein auto-regressive models for modeling multivariate distributional time series

Yiye Jiang \*

Université Grenoble Alpes, CNRS, Inria, Grenoble INP, LJK.

and

Jérémie Bigot

Institut de Mathématiques de Bordeaux, Université de Bordeaux

February 4, 2025

## Abstract

This paper is focused on the statistical analysis of data consisting of a collection of multiple series of probability measures that are indexed by distinct time instants and supported over a bounded interval of the real line. By modeling these time-dependent probability measures as random objects in the Wasserstein space, we propose a new auto-regressive model for the statistical analysis of multivariate distributional time series. Using the theory of iterated random function systems, results on the existence, uniqueness and stationarity of the solution of such a model are provided. We also propose a consistent estimator for the auto-regressive coefficients of this model. Due to the simplex constraints that we impose on the model coefficients, the proposed estimator that is learned under these constraints, naturally has a sparse structure. The sparsity allows the application of the proposed model in learning a graph of temporal dependency from multivariate distributional time series. We explore the numerical performances of our estimation procedure using simulated data. To shed some light on the benefits of our approach for real data analysis, we also apply this methodology to two data sets, respectively made of observations from age distribution in different countries and those from the bike sharing network in Paris.

*Keywords:* Wasserstein spaces; distributional data analysis; time series analysis; auto-regressive models; graph learning

*MSC Codes:* 62M10; 62H99; 62F10; 62F12.

---

\*This author is supported by MIAI@Grenoble Alpes, (ANR-19-P3IA-0003). Part of the work of this author was conducted while she was preparing her PhD at Université de Bordeaux.

# 1 Introduction

Distributional time series is a recent research field that deals with observations that can be modeled as sequences of time-dependent probability distributions. Such distributional time series are ubiquitous in many scientific fields. A pertinent example is the analysis of sequences of the indicator distributions supported over age intervals, such as mortality and fertility [Mazzuco and Scarpa, 2015, Shang and Haberman, 2020], over calendar years in demographic studies. Other examples include daily stock return distributions from financial time series [Kokoszka et al., 2019, Zhang et al., 2021], the distributions of correlations between pairs of voxels within brain regions [Petersen and Müller, 2016]. Figure 1 displays an illustrative example, a dataset made of time series of age distributions for countries in the European Union.

Probability distributions can be characterized by functions, such as densities, quantile functions, and cumulative distribution functions. Therefore, to analyze distributional time series, one may study one of its functional representations using tools from functional time series analysis [Bosq, 2000]. However, due to their nonlinear constraints, such as monotonicity and positivity, the representing functions of distributions do not constitute linear spaces. Consequently, basic notions in standard vector auto-regressive (VAR) models [Helmut, 2005], such as additivity and scalar multiplication, do not adapt, in a straightforward manner for random elements not belonging to a Hilbert space. An existing approach is to map the densities of distributions to unconstrained functions in the Hilbert space by the log quantile density (LQD) transformation [Petersen and Müller, 2016], and then to apply functional data analysis [Kokoszka et al., 2019]. However LQD does not take into account the geometry of the space of probability distributions, and recent approaches naturally turn to the development of time series models in the Wasserstein space.

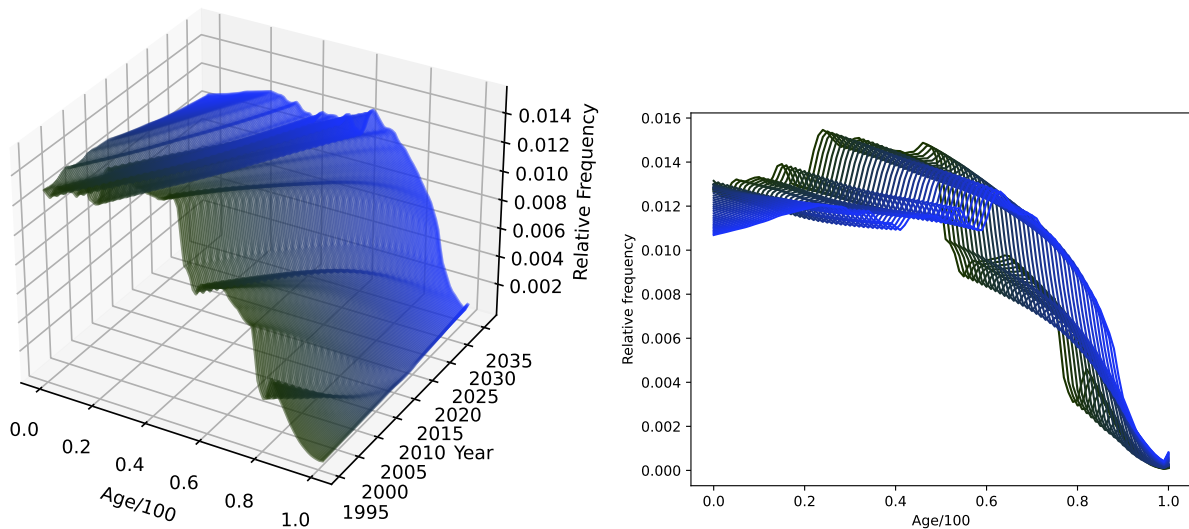
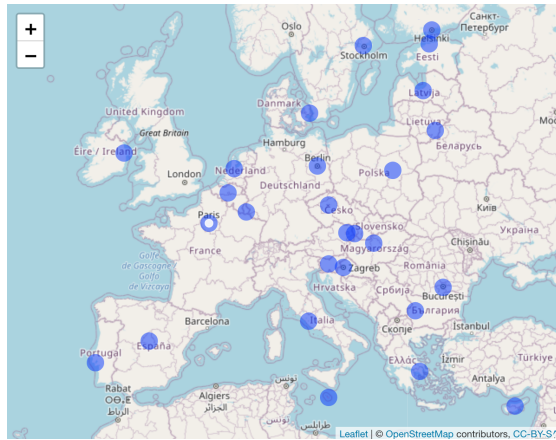


Figure 1: *Annual records of age distributions of EU countries.* On the top are 27 countries in the European union. A sequence of age distribution is recorded at each country over years. For example, at the bottom we illustrate the sequence of France, where one distribution supported over  $[0, 1]$  is observed at each year. On the lower left, we visualize the resulting univariate distributional time series with a surface in the coordinate system of Age  $\times$  Year  $\times$  Relative frequency. The raw data in this plot consist in 40 annual distributions. We complete them with interpolated samples to draw the surface. On the lower right, we show the projection of the raw time series onto the Age  $\times$  Relative frequency plane. We can see that the population is aging along time.

When observing a single distributional time series supported over an interval in  $\mathbb{R}$ , there exist recent works [Chen et al. \[2019\]](#), [Ghodrati and Panaretos \[2022b\]](#), [Chen et al. \[2021\]](#), [Zhang et al. \[2021\]](#), [Zhu and Müller \[2023a\]](#) on the development of stochastic models that extend the standard auto-regressive model to its distributional counterpart, based on the geometry of Wasserstein space. However, to the best of our knowledge, the development of multivariate auto-regressive dedicated to the analysis of multiple distributional time series, such as those displayed in [Figure 1](#), has not been considered so far. As for the regression models in Wasserstein space, similarly to the situation of auto-regressive models, almost all the existing tools consider only one predictor distribution (see for example [Ghodrati and Panaretos \[2022a\]](#)). One recent work devised for multiple predictor distributions is [Zhu and Müller \[2023b\]](#). They propose to rely only on optimal transport maps and a sequence of pushforwards to construct the regression. Such intrinsic method in the multivariate case will lead to an ordering problem, because pushing forward with the same set of transport maps but in different orders will give different distributions. To avoid such challenge, we propose to rely on the tangent space, where the addition is well defined between tangent vectors (essentially transport maps).

## 1.1 Main contributions

In this paper, we introduce a new auto-regressive model for the statistical analysis of multivariate distributional time series. The properties of this model can be analyzed thank to the theory of iterated random function systems [Wu and Shao \[2004\]](#), [Zhu and Müller \[2023a\]](#). Moreover, due to the geometric constraints inherited from the Wasserstein space that are imposed on the auto-regressive coefficients of the model, the estimator that we propose naturally has a sparse structure. In particular, this allows the application of our

approach to learning a sparse graph of temporal dependency from multivariate distributional time series. The numerical performances of our approach are then illustrated with simulated data. Finally, the methodology is applied to the real data set of age distribution displayed in Figure 1, in addition, to another real data set based on the bike-sharing network in Paris.

## 1.2 Organization of the paper

In Section 2, we provide the background on the geometry of the Wasserstein space. In Section 3, we introduce Wasserstein auto-regressive models that are adapted to the statistical analysis of multivariate distributional time series. We also prove the existence, uniqueness and stationarity of the solution of such models. Estimators of the auto-regressive coefficients coefficients in these models are then studied in Section 4. Finally, numerical experiments with using simulated and real data are carried out in Section 5 to analyze the finite sample properties of the estimator, and to illustrate its application in graph learning from multivariate distributional time series.

## 1.3 Publicly available source code

For the sake of reproducible research, Python code available at

[https://github.com/yiyej/Wasserstein\\_Multivariate\\_Autoregressive\\_Model](https://github.com/yiyej/Wasserstein_Multivariate_Autoregressive_Model)

implements the proposed estimators and the experiments carried out in this paper.

# 2 Background on the Wasserstein space

In this section, we present the background for modeling the distributional data considered in this work. Let  $\mathcal{D}$  be a bounded interval in  $\mathbb{R}$ , and  $\mathcal{B}(\mathcal{D})$  the associated  $\sigma$ -algebra made

of Borel subsets of  $\mathcal{D}$ . Without loss of generality, we assume that  $\mathcal{D} = [0, 1]$ . Let  $\mu$  be a probability measure (namely a distribution) over  $(\mathcal{D}, \mathcal{B}(\mathcal{D}))$  with cumulative distribution function (cdf)  $F_\mu$ . Then the (generalized) quantile function is defined as the left continuous inverse of  $F_\mu$ , denoted by  $F_\mu^{-1}$ , that is

$$F_\mu^{-1}(p) := \inf\{x \in \mathcal{D} : F_\mu(x) \geq p\}, \quad p \in (0, 1).$$

The Wasserstein space  $\mathcal{W} := \mathcal{W}_2(\mathcal{D})$  is defined as the set of probability measures over  $(\mathcal{D}, \mathcal{B}(\mathcal{D}))$  with finite second moment, that is endowed with the  $\mathcal{L}^2$  Wasserstein distance

$$d_W(\mu, \nu) = \left( \int_0^1 [F_\mu^{-1}(p) - F_\nu^{-1}(p)]^2 dp \right)^{1/2}, \quad \mu, \nu \in \mathcal{W}_2(\mathcal{D}). \quad (2.1)$$

It is well known that  $\mathcal{W}$  is a complete and separable metric space (see e.g. [Villani \[2021\]](#) for a detailed course on optimal transport theory and [Panaretos and Zemel \[2020\]](#) for an introduction to the topic of statistical analysis in the Wasserstein space).

## 2.1 Tangent Bundle

The space  $\mathcal{W}$  has a pseudo-Riemannian structure as shown in [Ambrosio et al. \[2008\]](#). Letting  $\gamma \in \mathcal{W}$  be an absolutely continuous measure, the tangent space at  $\gamma$  is defined as

$$\text{Tan}_\gamma = \overline{\{t(F_\mu^{-1} \circ F_\gamma - id) : \mu \in \mathcal{W}, t > 0\}}^{\mathcal{L}_\gamma^2(\mathcal{D})},$$

where  $id$  is the identity function,  $\mathcal{L}_\gamma^2(\mathcal{D})$  is the Hilbert space of  $\gamma$  square integrable functions on  $\mathcal{D}$ , with inner product  $\langle \cdot, \cdot \rangle_\gamma$  defined by  $\langle f, g \rangle_\gamma := \int_{\mathcal{D}} f(x)g(x) d\gamma(x)$ ,  $f, g \in \mathcal{L}_\gamma^2(\mathcal{D})$ , and the induced norm  $\| \cdot \|_\gamma$ . The exponential and the logarithmic maps at  $\gamma$  are then defined as follows.

**Definition 2.1.** *The exponential map  $\text{Exp}_\gamma : \text{Tan}_\gamma \rightarrow \mathcal{W}$  is defined as*

$$\text{Exp}_\gamma g = (g + id) \# \gamma, \quad (2.2)$$

where for any measurable function  $T : \mathcal{D} \rightarrow \mathcal{D}$  and  $\mu \in \mathcal{W}$ ,  $T\#\mu$  is the pushforward measure on  $\mathcal{D}$  defined as  $T\#\mu(A) = \mu(\{x \in \mathcal{D} : T(x) \in A\})$ , for any set  $A \in \mathcal{B}(\mathcal{D})$ .

**Definition 2.2.** The logarithmic map  $\text{Log}_\gamma : \mathcal{W} \rightarrow \text{Tan}_\gamma$  is defined as

$$\text{Log}_\gamma \mu = F_\mu^{-1} \circ F_\gamma - \text{id}.$$

When restricted to the image of the logarithmic map, the exponential map (2.2) becomes an isometry [Bigot et al., 2017] as stated in the following proposition.

**Proposition 2.1.** Let  $\gamma \in \mathcal{W}$  be any absolutely continuous measure. Then  $\text{Exp}_\gamma|_{\text{Log}_\gamma \mathcal{W}}$  is an isometric homeomorphism from  $\text{Log}_\gamma \mathcal{W}$  to  $\mathcal{W}$ , with the inverse map  $\text{Log}_\gamma$ , satisfying

$$d_W(\mu, \nu) = \|\text{Log}_\gamma \mu - \text{Log}_\gamma \nu\|_\gamma.$$

We recall below some important properties of  $\text{Log}_\gamma \mathcal{W}$  [Bigot et al., 2017] that are needed in the construction of the statistical models introduced in Section 3.

**Proposition 2.2.**  $\text{Log}_\gamma \mathcal{W}$  is a closed and convex subset of  $\mathcal{L}_\gamma^2(\mathcal{D})$ .

**Proposition 2.3.** Let  $g \in \text{Tan}_\gamma$ , then  $g \in \text{Log}_\gamma \mathcal{W}$  if and only if  $g + \text{id}$  is nondecreasing  $\gamma$ -almost everywhere.

## 2.2 Fréchet Mean in the Wasserstein space

**Definition 2.3.** Let  $\mu_1, \dots, \mu_T$  be probability measures in  $\mathcal{W}$ . The empirical Fréchet mean of  $\mu_1, \dots, \mu_T$ , denoted by  $\bar{\mu}$ , is defined as the unique minimizer of

$$\min_{\nu \in \mathcal{W}} \frac{1}{T} \sum_{t=1}^T d_W^2(\mu_t, \nu).$$

It is well known that the empirical Fréchet mean  $\bar{\mu}$  admits a simple expression through its quantile function that satisfies

$$F_{\bar{\mu}}^{-1}(p) = \frac{1}{T} \sum_{t=1}^T F_{\mu_t}^{-1}(p), \quad p \in (0, 1).$$

**Definition 2.4.** A random measure  $\boldsymbol{\mu}$  is any measurable map from a probability space  $(\Omega, \mathcal{F}, \mathbb{P})$  to the metric space  $\mathcal{W}$ , endowed with its Borel  $\sigma$ -algebra.

In what follows, we use bold notation to distinguish random measures from constant (that is non-random) measures.

**Definition 2.5.** Let  $\boldsymbol{\mu}$  be a random measure from a probability space  $(\Omega, \mathcal{F}, \mathbb{P})$  to  $\mathcal{W}$ . Assume that  $\boldsymbol{\mu}$  is square integrable, namely  $\mathbb{E}d_{\mathcal{W}}^2(\boldsymbol{\mu}, \nu) < \infty$  for some (thus for all)  $\nu \in \mathcal{W}$ . Then, the population Fréchet mean of  $\boldsymbol{\mu}$ , denoted by  $\mu_{\oplus}$ , is defined as the unique minimizer of

$$\min_{\nu \in \mathcal{W}} \mathbb{E} [d_{\mathcal{W}}^2(\boldsymbol{\mu}, \nu)].$$

Note that  $\mu_{\oplus}$  also admits a simple expression through its quantile function as

$$F_{\mu_{\oplus}}^{-1}(p) = \mathbb{E} [F_{\boldsymbol{\mu}}^{-1}(p)], \quad p \in (0, 1).$$

### 3 Wasserstein multivariate auto-regressive Models

In this section, we consider data that are collected over a network of  $N$  sensors (typically a set of spatial locations), recording, over time, observations of multiple measurements. Standard VAR models are adapted to the case where real measurements  $\boldsymbol{x}_t^i \in \mathbb{R}$ ,  $i = 1, \dots, N$  are collected for each sensor  $i$  and time  $t$ . In this work, we focus on the more involved setting of multivariate distributional time series. This corresponds to the situation where one records, for each sensor  $i$  and time  $t$ , a probability measure  $\boldsymbol{\mu}_t^i$  supported on  $\mathcal{D}$ . Hence, we observe a collection of  $N$  time-dependent probability measures  $(\boldsymbol{\mu}_t^i)_{t \in \mathbb{Z}}$  for  $i = 1, \dots, N$  that are indexed by distinct time instants  $t$ . The purpose of this section is then to extend standard VAR models to analyse such data, and to propose an estimation of the dependency structure in the temporal evolution of the measures.



### 3.1 Description of the model

We first recall the standard VAR model. Then, we generalize it to multivariate distributional time series to develop a new notion of multivariate distributional auto-regressive model.

Given a multivariate time series  $\mathbf{x}_t^i \in \mathbb{R}$ ,  $t \in \mathbb{Z}$ ,  $i = 1, \dots, N$ , such that the expectation is time invariant for each component  $i$  that is  $u^i = \mathbb{E}(\mathbf{x}_t^i)$ ,  $t \in \mathbb{Z}$ . Then the VAR model of order 1 (not including an intercept term) writes as [Helmut \[2005\]](#)

$$\mathbf{x}_t^i - u_i = \sum_{j=1}^N A_{ij}(\mathbf{x}_{t-1}^j - u_j) + \boldsymbol{\epsilon}_t^i, \quad (3.1)$$

where  $\boldsymbol{\epsilon}_t^i$  is a white noise.

For the multivariate distributional time series  $\boldsymbol{\mu}_t^i$ ,  $t \in \mathbb{Z}$ ,  $i = 1, \dots, N$ , we firstly assume that the Fréchet mean is time invariant for each component  $i$  as well, as stated in Assumption [A1](#) below.

**Assumption A1.** *For each fixed  $i = 1, \dots, N$ , the random probability measures  $\boldsymbol{\mu}_t^i$ ,  $t \in \mathbb{Z}$  are square integrable and they have the same Fréchet mean denoted by  $\mu_{i,\oplus}$ . Moreover, we assume that the cdf  $\mathbf{F}_{i,t}$  of  $\boldsymbol{\mu}_t^i$  is strictly increasing and continuous for each  $t \in \mathbb{Z}$ ,  $i = 1, \dots, N$ .*

We then propose the following “data centering step” for  $\boldsymbol{\mu}_t^i$ ,  $t \in \mathbb{Z}$ ,  $i = 1, \dots, N$ . The centered measures are denoted by  $\tilde{\boldsymbol{\mu}}_t^i$ , and they are defined through their quantile functions given as

$$\tilde{\mathbf{F}}_{i,t}^{-1} = \mathbf{F}_{i,t}^{-1} \ominus F_{i,\oplus}^{-1} := \mathbf{F}_{i,t}^{-1} \circ F_{i,\oplus}, \quad (3.2)$$

where  $\mathbf{F}_{i,t}^{-1}$  is the quantile function of  $\boldsymbol{\mu}_t^i$  extended at 0 [[Bobkov and Ledoux, 2014](#), Section [A1](#)] by

$$\mathbf{F}_{i,t}^{-1}(0) := \inf\{x \in [0, 1] : \mathbf{F}_{i,t}(x) > 0\},$$

$F_{i,\oplus}^{-1}$  and  $F_{i,\oplus}$  are respectively the quantile function and the cdf of  $\mu_{i,\oplus}$ .

The centering step (3.2) at the level of the quantile functions is thus analogous to the usual centering step in VAR models for Euclidean data. From the optimal transport point of view, the centered quantile function  $\tilde{F}_{i,t}^{-1}$  is interpreted as the optimal transport map from the Fréchet mean  $\mu_{i,\ominus}$  to the measure  $\mu_t^i$ . The notation  $\ominus$  in (3.2) as a difference operator between two increasing functions is taken from the recent work in [Zhu and Müller \[2023a\]](#) on auto-regressive model for univariate (that is  $N = 1$ ) distributional time series.

Now, we remark that

$$\mathbb{E} \left[ \tilde{F}_{i,t}^{-1}(p) \right] = (\mathbb{E} F_{i,t}^{-1}) [F_{i,\ominus}(p)] = p, \quad p \in (0, 1). \quad (3.3)$$

Thus, all the centered distributional time series  $(\tilde{\mu}_t^i)_{t \in \mathbb{Z}}$  have the same Fréchet mean that equals to the Lebesgue measure on  $\mathcal{D} = [0, 1]$ . We illustrate this centering step with synthetic data in [Figure 2](#), where it can be seen that the centered measures have empirical Fréchet mean that equals the Lebesgue measure.

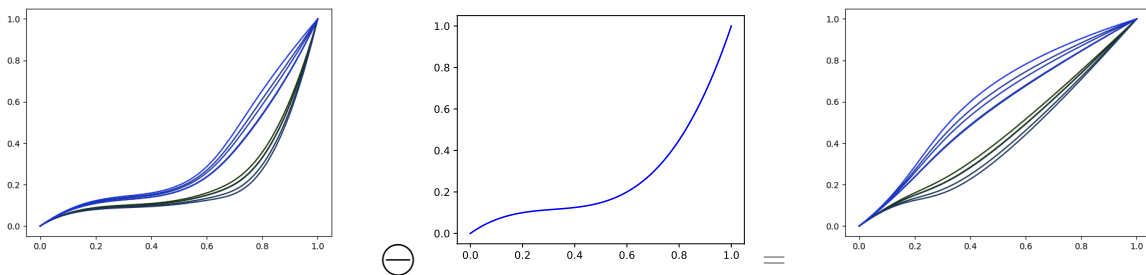


Figure 2: *Centering of a random probability measure.* On the left, we display i.i.d. samples of a random probability measure, whose population Fréchet mean is given in the middle. Applying the centering step (3.2) on them gives the centred samples shown on the right. All probability measures are represented by their quantile functions.

We then propose to build an auto-regressive model for multivariate distributional time series with respect to the transformed data  $\tilde{\mu}_t^i$  in the tangent space of the Lebesgue measure,

that takes the following expression:

$$\tilde{\boldsymbol{\mu}}_t^i = \boldsymbol{\epsilon}_{i,t} \# \text{Exp}_{Leb} \left( \sum_{j=1}^N A_{ij} \text{Log}_{Leb} \tilde{\boldsymbol{\mu}}_{t-1}^j \right), \quad t \in \mathbb{Z}, i = 1, \dots, N, \quad (3.4)$$

where  $\{\boldsymbol{\epsilon}_{i,t}\}_{i,t}$  are i.i.d. random<sup>1</sup> distortion functions taking values in the space of extended quantile functions

$$\Pi = \{F^{-1} : [0, 1] \rightarrow [0, 1], \text{ such that } F^{-1}|_{(0,1)} \in \text{Log}_{Leb} \mathcal{W} + id,$$

$$F^{-1}(0) := \inf\{x \in [0, 1] : F(x) > 0\}, \text{ and } F^{-1}(1) := \sup\{x \in [0, 1] : F(x) < 1\}\},$$

endowed with  $\|\cdot\|_{Leb}$  and the induced Borel algebra,  $\boldsymbol{\epsilon}_{i,t}$  is almost surely independent of  $\boldsymbol{\mu}_{t-1}^i, i = 1, \dots, N$ , for all  $t \in \mathbb{Z}$ , and

$$\mathbb{E}[\boldsymbol{\epsilon}_{i,t}(x)] = x, x \in [0, 1].$$

Note that all the univariate time series of log maps are centered to 0, namely,  $\mathbb{E}[\text{Log}_{Leb} \tilde{\boldsymbol{\mu}}_t^i] = 0, \forall t \in \mathbb{Z}, i = 1, \dots, N$  as in Model (3.1).

The pushforward in (3.4) under  $\boldsymbol{\epsilon}_{i,t}$  is a valid approach to provide random distortions of probability measures as proposed in Petersen and Müller [2019a]. This approach is also used in Chen et al. [2021]. An example of random distortion function satisfying the conditions in Equation (3.4) as well as in Assumption A3 imposed later on, can be found, for example in [Chen et al., 2021, Equation (38)]. However, in these works, not many examples of valid random distortion functions which satisfy the conditions in Equation (3.4) are given. Thus, to demonstrate that the conditions imposed on the distortion function are not restrictive, we describe, in Section 5 on numerical experiments, a general mechanism to generate random distortion functions that satisfy both Equation (3.4) and Assumption A3.

Note that, the coefficients of the Wasserstein auto-regressive Model (3.4) defines a matrix  $A = (A_{ij})_{ij}$  as in VAR models. To fit Model (3.4), a least squares estimator of the matrix  $A$

---

<sup>1</sup>We do not consider degenerate distributions.

can be constructed by minimizing the expected squared Wasserstein distance (2.1) between  $\tilde{\boldsymbol{\mu}}_t^i$  and its prediction  $\text{Exp}_{Leb} \left( \sum_{j=1}^N A_{ij} \text{Log}_{Leb} \tilde{\boldsymbol{\mu}}_{t-1}^j \right)$ . Note that when  $\sum_{j=1}^N A_{ij} \text{Log}_{Leb} \tilde{\boldsymbol{\mu}}_t^{j-1}$  belongs to  $\text{Log}_{Leb} \mathcal{W}$ , the quantile function of its Exponential map  $\text{Exp}_{Leb}$  is simply given by  $\sum_{j=1}^N A_{ij} \left( \tilde{\mathbf{F}}_{j,t-1}^{-1} - id \right) + id$ . By contrast, when  $\sum_{j=1}^N A_{ij} \text{Log}_{Leb} \tilde{\boldsymbol{\mu}}_t^{j-1}$  falls out of  $\text{Log}_{Leb} \mathcal{W}$ , the dependency between the quantile function and the coefficients  $A_{ij}$  is non-tractable, see [Cazelles et al., 2017, Proposition 3.1]. On the other hand, constraining this sum to belong to  $\text{Log}_{Leb} \mathcal{W}$  avoids the non-identifiability problem of parametric models, thanks to Proposition 2.1.

Thus, we further need that  $\sum_{j=1}^N A_{ij} \text{Log}_{Leb} \tilde{\boldsymbol{\mu}}_t^{j-1} \in \text{Log}_{Leb} \mathcal{W}$ . Since  $\tilde{\boldsymbol{\mu}}_t^{j-1}$  can take any value in  $\mathcal{W}$ , imposing such assumption amounts to the following  $N$ -simplex constraint on the rows of  $A$ , given the convexity of the logarithmic image. Similar assumptions are imposed in related works, see e.g. [Chen et al., 2021, Assumption (A1)] and [Petersen and Müller, 2019b, Assumption (A3)], to keep the regression model in the logarithmic image.

**Assumption A2.**  $\sum_{j=1}^N A_{ij} \leq 1$  and  $0 \leq A_{ij} \leq 1$ .

A key advantage of Assumption A2 is that it leads to least squares estimation of the matrix  $A$  under an  $\ell_1$  ball constraint on its coefficients. In this manner, the estimators of the coefficients  $A_{ij}$  will naturally be sparse, which is a favorable property in graph learning, where  $A$  is considered as an adjacency matrix.

Given Assumption A2, it follows that the auto-regressive Model (3.4) writes with respect to the quantile function  $\tilde{\mathbf{F}}_{i,t}^{-1}$  as

$$\tilde{\mathbf{F}}_{i,t}^{-1} = \boldsymbol{\epsilon}_{i,t} \circ \left[ \sum_{j=1}^N A_{ij} \left( \tilde{\mathbf{F}}_{j,t-1}^{-1} - id \right) + id \right], \quad t \in \mathbb{Z}, i = 1, \dots, N. \quad (3.5)$$

When reducing to the univariate case ( $N = 1$ ), Model (3.5) is similar to the auto-regressive model proposed in [Zhu and Müller, 2023a, Model (4)], when a regression coefficient is constrained to belong to  $(0, 1]$ .

## 3.2 Existence, uniqueness and stationarity

To study the legitimacy of the iterated random functions (IRF) system defined by Model (3.5), we shall consider the product metric space

$$(\mathcal{X}, d) := (\mathcal{T}, \|\cdot\|_{Leb})^{\otimes N},$$

where  $\mathcal{T} := \text{Log}_{Leb} \mathcal{W} + id$  is the space of all quantile functions of  $\mathcal{W}$ , equipped with the norm  $\|\cdot\|_{Leb}$  in the tangent space at the Lebesgue measure. Thus, we have

$$d(\mathbf{X}, \mathbf{Y}) := \sqrt{\sum_{i=1}^N \|\mathbf{X}_i - \mathbf{Y}_i\|_{Leb}^2}, \quad \mathbf{X} = (\mathbf{X}_i)_{i=1}^N \in \mathcal{X}, \quad \mathbf{Y} = (\mathbf{Y}_i)_{i=1}^N \in \mathcal{X}.$$

The auto-regressive model (3.5) can be interpreted as an iterated random functions (IRF) system operating on the state space  $(\mathcal{X}, d)$ , written as

$$\mathbf{X}_t = \Phi_{\epsilon_t}(\mathbf{X}_{t-1}), \tag{3.6}$$

where  $\mathbf{X}_t = (\mathbf{X}_{i,t})_{i=1}^N$ ,  $\epsilon_t = (\epsilon_{i,t})_{i=1}^N$ , and  $\Phi_{\epsilon_t}(\mathbf{X}_{t-1}) = (\Phi_{\epsilon_t}^i(\mathbf{X}_{t-1}))_{i=1}^N$  with

$$\Phi_{\epsilon_t}^i(\mathbf{X}_{t-1}) := \epsilon_{i,t} \circ \left[ \sum_{j=1}^N A_{ij}(\mathbf{X}_{j,t-1} - id) + id \right].$$

We first study the existence and the uniqueness of the solution to the IRF system in the metric space  $(\mathcal{X}, d)$ .

For time series models in a Hilbert space, two standard assumptions that ensure the existence and the uniqueness of the solutions are the boundedness of the  $L_p$  norm of random additive noise and the contraction of the regression operator. For Model (3.6), the random noise  $\epsilon_{i,t}$  is bounded between 0 and 1, and thus  $\mathbb{E}[d^p(\mathbf{X}, \epsilon)]$  is bounded for all  $\mathbf{X} \in \mathcal{X}$ , which is the  $L_p$  norm equivalent condition in the metric space setting. Then, to have a contractive map  $\Phi_{\epsilon_t}$ , we shall rely on an interplay between properties of the matrix  $A$  of coefficients and the random noise distortion since it is applied in a nonlinear way. More specifically, we impose Assumptions A3 and A4 below on Model (3.6).

**Assumption A3.** *There exists a constant  $L > 0$  such that  $\mathbb{E}[\epsilon_{i,t}(x) - \epsilon_{i,t}(y)]^2 \leq L^2(x - y)^2$ ,  $\forall x, y \in [0, 1]$ ,  $t \in \mathbb{Z}$ ,  $i = 1, \dots, N$ ,*

**Assumption A4.** *The matrix of auto-regressive coefficients satisfies  $\|A\|_2 < \frac{1}{L}$ , where  $L$  is the Lipschitz constant from Assumption A3.*

Note that, Assumption A3 implies that  $\epsilon_{i,t}$  is  $L$ -Lipschitz in expectation. For increasing functions from  $[0, 1]$  to  $[0, 1]$ , the smallest value of  $L$  is 1 that is attained by the identity function. Therefore, Assumption A4 implies that  $\|A\|_2 < 1$ , which is the usual contraction assumption for standard VAR models in an Euclidean space. We now state the existence and uniqueness results.

**Theorem 3.1.** *Under Assumptions A2, A3 and A4, the IRF system (3.6) almost surely admits a solution  $\mathbf{X}_t$ ,  $t \in \mathbb{Z}$ , with the same marginal distribution  $\pi$ , namely,  $\mathbf{X}_t \stackrel{d}{=} \pi$ ,  $\forall t \in \mathbb{Z}$ , where the notation  $\stackrel{d}{=}$  means equality in distribution. Moreover, if there exists another solution  $\mathbf{S}_t$ ,  $t \in \mathbb{Z}$ , then for all  $t \in \mathbb{Z}$*

$$\mathbf{X}_t \stackrel{d}{=} \mathbf{S}_t, \text{ almost surely.}$$

Theorem 3.1 states that under Assumptions A3 and A4, a well defined IRF system (3.6) (namely when Assumption A2 is satisfied) permits a unique solution in  $(\mathcal{X}, d)$  almost surely. Next, we show that this solution is furthermore stationary as a functional time series in a Hilbert space. To this end, we need to assume that there is an underlying Hilbert space associated to  $(\mathcal{X}, d)$ , with  $\mathcal{X}$  its subset and  $d$  equal to the induced norm of its inner product. Such Hilbert space exists

$$(\text{Tan}_{Leb} + id, \langle, \rangle_{Leb})^{\otimes N}.$$

Thus we have  $\langle X, Y \rangle = \sum_{i=1}^N \langle X_i, Y_i \rangle_{Leb}$ ,  $X, Y \in (\text{Tan}_{Leb} + id, \langle, \rangle_{Leb})^{\otimes N}$ .

We recall the conventional definition of weak stationarity for process in a separable Hilbert space, see for example [Zhang et al., 2021, Definition 2.2]. We recall the definition

**Definition 3.1.** *A random process  $\{\mathbf{V}_t\}_t$  in a separable Hilbert space  $(\mathcal{H}, \langle \cdot, \cdot \rangle)$  is said to be stationary if the following properties are satisfied.*

1.  $\mathbb{E} \|\mathbf{V}_t\|^2 < \infty$ .
2. The Hilbert mean  $U := \mathbb{E} [\mathbf{V}_t]$  does not depend on  $t$ .
3. The auto-covariance operators defined as

$$\mathcal{G}_{t,t-h}(V) := \mathbb{E} \langle \mathbf{V}_t - U, V \rangle (\mathbf{V}_{t-h} - U), \quad V \in \mathcal{H},$$

do not depend on  $t$ , that is  $\mathcal{G}_{t,t-h}(V) = \mathcal{G}_{0,-h}(V)$  for all  $t$ .

Then, Theorem 3.2 below gives the stationarity result.

**Theorem 3.2.** *The unique solution given in Theorem 3.1 is stationary as a random process in  $(\mathcal{X}, \langle \cdot, \cdot \rangle)$  in the sense of Definition 3.1.*

Besides, Proposition 3.3 below states that the stationary solution of the IRF system (3.6) satisfies the property (3.3) of the transformed series  $\tilde{\mathbf{F}}_{i,t}^{-1}, t \in \mathbb{Z}$ . Thus, it is consistent to propose the IRF system (3.6) as the process that generated the data  $\tilde{\mathbf{F}}_{i,t}^{-1}$ , which completes the building of Model (3.5) as valid approach to analyze multivariate distributional time series.

**Proposition 3.3.** *The stationary solution  $\mathbf{X}_t$  of the IRF system (3.6) satisfies:*

1.  $\mathbf{X}_{i,t}(p) \in [0, 1], \quad \forall p \in (0, 1),$
2.  $\mathbb{E} [\mathbf{X}_{i,t}(p)] = p, \quad \forall p \in (0, 1).$

3.  $\mathbb{E} [\mathbf{X}_{i,t}(x) - \mathbf{X}_{i,t}(y)]^2 \leq C(L)^2(x-y)^2, \forall x, y \in [0, 1], \quad t \in \mathbb{Z}, i = 1, \dots, N,$  with  $C(L)$  a constant depending on  $L$ , the lipschitz constant defined in Assumption A3.

Finally, we point out in Proposition 3.4 additional properties of the IRF system (3.6) that will serve in the following section of the estimation of the matrix of coefficients in Model (3.5).

**Proposition 3.4.** *Given the stationary solution  $\mathbf{X}_t$  of the IRF system (3.6), we define matrices  $\Gamma(0), \Gamma(1) \in \mathbb{R}^{N \times N}$  as*

$$\begin{aligned} [\Gamma(0)]_{j,l} &= \mathbb{E} \langle \mathbf{X}_{j,t-1} - id, \mathbf{X}_{l,t-1} - id \rangle_{Leb} \\ [\Gamma(1)]_{j,l} &= \mathbb{E} \langle \mathbf{X}_{j,t} - id, \mathbf{X}_{l,t-1} - id \rangle_{Leb}, \end{aligned}$$

for  $1 \leq j, l \leq N$ . We have

1.  $\Gamma(0)$  is nonsingular,
2. the coefficient matrix  $A$  of the IRF system (3.6) admits the representation

$$A = \Gamma(1) [\Gamma(0)]^{-1}. \tag{3.7}$$

Note that the expression (3.7) for the matrix  $A$  is analogous to the one of VAR models with matrices  $\Gamma(0), \Gamma(1)$  carrying out the information on the correlation. However, compared to the auto-covariance operators in Definition 3.1, the matrices  $\Gamma(0)$  and  $\Gamma(1)$  rather reflect the average auto-covariance taking into account additionally the correlated level along the function domain.

## 4 Estimation of the regression coefficients

In this section, we develop the estimators of coefficient  $A$ , given  $T + 1$  samples  $\boldsymbol{\mu}_t^i, t = 0, 1, \dots, T$  for each sensor  $i = 1, \dots, N$ . We also show the consistency result of the proposed



estimator. Note that we assume that the measures are fully observed, instead of indirectly observed through their samples.

## 4.1 A constrained least-square estimation method

As briefly explained before the statement of Assumption A2, we could consider the estimator based on an unconstrained least squares method, which is defined as the minimizer of the sum of squared residuals measured by the Wasserstein distance:

$$\begin{aligned} \tilde{\mathbf{A}}_i &= \arg \min_{A_{i:}} \frac{1}{T} \sum_{t=1}^T d_W^2 \left[ \tilde{\boldsymbol{\mu}}_t^i, \text{Exp}_{Leb} \left( \sum_{j=1}^N A_{ij} \text{Log}_{Leb} \tilde{\boldsymbol{\mu}}_t^{j-1} \right) \right], \quad i = 1, \dots, N, \\ &= \arg \min_{A_{i:}} \frac{1}{T} \sum_{t=1}^T \left\| \tilde{\mathbf{F}}_{i,t}^{-1} - \sum_{j=1}^N A_{ij} \left( \tilde{\mathbf{F}}_{j,t-1}^{-1} - id \right) - id \right\|_{Leb}^2, \quad i = 1, \dots, N, \end{aligned} \quad (4.1)$$

Analogous to Proposition 3.4, the estimator  $\tilde{\mathbf{A}}$  defined in Equation (4.1) admits the expression

$$\tilde{\mathbf{A}} = \tilde{\mathbf{\Gamma}}(1) \left[ \tilde{\mathbf{\Gamma}}(0) \right]^{-1},$$

where

$$\left[ \tilde{\mathbf{\Gamma}}(0) \right]_{j,l} = \frac{1}{T} \sum_{t=1}^T \langle \tilde{\mathbf{F}}_{j,t-1}^{-1} - id, \tilde{\mathbf{F}}_{l,t-1}^{-1} - id \rangle_{Leb}$$

and

$$\left[ \tilde{\mathbf{\Gamma}}(1) \right]_{j,l} = \frac{1}{T} \sum_{t=1}^T \langle \tilde{\mathbf{F}}_{j,t}^{-1} - id, \tilde{\mathbf{F}}_{l,t-1}^{-1} - id \rangle_{Leb}.$$

For the estimator  $\tilde{\mathbf{A}}$  to hold, strictly speaking, we need to assume that  $\tilde{\mathbf{\Gamma}}(0)$  is nonsingular as in the case of classical least squares estimators.

Note that  $\tilde{\mathbf{A}}$  is the exact least squares estimator constructed from the stationary solution of Model (3.5) without any constraint. However, in practice, we do not know the population Fréchet mean  $F_{i,\oplus}^{-1}$ , thus we can not calculate the exact centered data  $\tilde{\boldsymbol{\mu}}_t^i$  as in method (3.2). Therefore, we propose to first estimate  $F_{i,\oplus}^{-1}$  by the empirical Fréchet mean

$$\mathbf{F}_{\tilde{\mu}_i}^{-1} = \frac{1}{T} \sum_{t=1}^T \mathbf{F}_{i,t}^{-1}, \quad (4.2)$$

and center  $\boldsymbol{\mu}_{i,t}$  by  $\mathbf{F}_{\bar{\mu}_i}^{-1}$  as in Equation (4.3), to obtain the transformed data  $\hat{\boldsymbol{\mu}}_{i,t}$ .

$$\hat{\mathbf{F}}_{i,t}^{-1} := \mathbf{F}_{i,t}^{-1} \ominus \mathbf{F}_{\bar{\mu}_i}^{-1} = \mathbf{F}_{i,t}^{-1} \circ \mathbf{F}_{\bar{\mu}_i}. \quad (4.3)$$

Using the data  $\hat{\boldsymbol{\mu}}_{i,t}$  in the least squares formula (4.1) we obtain an approximate least squares estimator  $\hat{\mathbf{A}}_o$  whose rows satisfy

$$\left[ \hat{\mathbf{A}}_o \right]_{i:} = \arg \min_{\mathbf{A}_{i:}} \frac{1}{T} \sum_{t=1}^T \left\| \hat{\mathbf{F}}_{i,t}^{-1} - \sum_{j=1}^N A_{ij} \left( \hat{\mathbf{F}}_{j,t-1}^{-1} - id \right) - id \right\|_{Leb}^2, \quad i = 1, \dots, N,$$

Analogously,

$$\hat{\mathbf{A}}_o = \hat{\mathbf{\Gamma}}(1) \left[ \hat{\mathbf{\Gamma}}(0) \right]^{-1}, \quad (4.4)$$

where

$$[\hat{\mathbf{\Gamma}}(0)]_{j,l} = \frac{1}{T} \sum_{t=1}^T \langle \hat{\mathbf{F}}_{j,t-1}^{-1} - id, \hat{\mathbf{F}}_{l,t-1}^{-1} - id \rangle_{Leb}$$

and

$$[\hat{\mathbf{\Gamma}}(1)]_{j,l} = \frac{1}{T} \sum_{t=1}^T \langle \hat{\mathbf{F}}_{j,t}^{-1} - id, \hat{\mathbf{F}}_{l,t-1}^{-1} - id \rangle_{Leb}.$$

As before, we assume that  $\hat{\mathbf{\Gamma}}(0)$  is invertible. Finally, we add the coefficient constraints to the problem, corresponding to the simplex constraint (A2). Therefore, the estimator  $\hat{\mathbf{A}}$  that we finally propose is defined as

$$\hat{\mathbf{A}}_{i:} = \arg \min_{\mathbf{A}_{i:} \in B_+^1} \frac{1}{T} \sum_{t=1}^T \left\| \hat{\mathbf{F}}_{i,t}^{-1} - \sum_{j=1}^N A_{ij} \left( \hat{\mathbf{F}}_{j,t-1}^{-1} - id \right) - id \right\|_{Leb}^2, \quad i = 1, \dots, N, \quad (4.5)$$

where  $B_+^1$  is  $N$ -dimensional simplex, that is the nonnegative orthant of the  $\ell_1$  unit ball  $B^1$  in  $\mathbb{R}^N$ . Thus, an important advantage of this constraint is to promote sparsity in  $\hat{\mathbf{A}}_{i:}$ , which will be illustrated in Section 5. The optimisation problem (4.5) can be solved by the accelerated projected gradient descent [Parikh and Boyd, 2014, Chapter 4.3]. The projection onto  $B_+^1$  is given in Thai et al. [2015].

## 4.2 Consistency of the estimators

Now, we study the consistency of the proposed estimator  $\hat{\mathbf{A}}$ . The main result of this section is Theorem 4.4. The details of its proof is given in the supplemental material. Instead, in this section, we resume the proof by the key intermediate results in its development.

The proof proceeds by firstly showing the consistency of the unconstrained least squares estimator  $\tilde{\mathbf{A}}$  (see Lemma 4.1) that uses the knowledge of the population Fréchet mean  $F_{i,\oplus}^{-1}$ . Secondly, we show the convergence on the empirical Fréchet mean  $\mathbf{F}_{\mu_i}^{-1}$  (see Lemma 4.2), and aim to rely on this result to prove that  $\hat{\mathbf{A}}_o - \tilde{\mathbf{A}} \xrightarrow{p} 0$  (see Theorem 4.3). Given the consistency of  $\hat{\mathbf{A}}_o$ , we lastly show the proposed estimator  $\hat{\mathbf{A}}$  is also consistent (see Theorem 4.4) as the constrained version of  $\hat{\mathbf{A}}_o$ . To this end, we apply a general result on the consistency of constrained estimators provided in the supplementary materials.

**Lemma 4.1.** *Assume that  $\mu_t^i$ ,  $i = 1, \dots, N$  satisfy Assumption A1 for  $t = 0, 1, \dots, T$ , and the transformed sequence  $\tilde{\mathbf{F}}_t^{-1}$ ,  $t = 0, 1, \dots, T$  satisfies Model (3.6) with Assumption A2 true. Suppose additionally that  $\tilde{\mathbf{F}}_0^{-1} \stackrel{d}{=} \pi$  with  $\pi$  the stationary distribution defined in Theorem 3.1. Given Assumptions A3 and A4 hold true, and  $\tilde{\Gamma}(0)$  is nonsingular, where we recall that  $\tilde{\Gamma}(0) \in \mathbb{R}^{N \times N}$  is defined as*

$$\left[ \tilde{\Gamma}(0) \right]_{j,l} = \frac{1}{T} \sum_{t=1}^T \langle \tilde{\mathbf{F}}_{j,t-1}^{-1} - id, \tilde{\mathbf{F}}_{l,t-1}^{-1} - id \rangle_{Leb},$$

we obtain

$$\tilde{\mathbf{A}} - A = \mathcal{O}_p\left(\frac{1}{\sqrt{T}}\right).$$

**Lemma 4.2.** *Under the conditions of Lemma 4.1, we have*

$$\frac{1}{T} \sum_{t=1}^T \tilde{\mathbf{F}}_{i,t-1}(p) - p = \mathcal{O}_p\left(\frac{1}{\sqrt{T}}\right), \quad \forall p \in (0, 1), \quad i = 1, \dots, N.$$

Since  $\tilde{\mathbf{F}}_{i,t}^{-1} = \mathbf{F}_{i,t}^{-1} \circ F_{i,\oplus}$ , we have equivalently,

$$\mathbf{F}_{\mu_i}^{-1}(p) - F_{i,\oplus}^{-1}(p) = \mathcal{O}_p\left(\frac{1}{\sqrt{T}}\right), \quad \forall p \in (0, 1), \quad i = 1, \dots, N.$$

**Theorem 4.3.** *Under the conditions of Lemma 4.1, and  $\widehat{\Gamma}(0)$  is nonsingular, where we recall*

$$[\widehat{\Gamma}(0)]_{j,l} = \frac{1}{T} \sum_{t=1}^T \langle \widehat{\mathbf{F}}_{j,t-1}^{-1} - id, \widehat{\mathbf{F}}_{l,t-1}^{-1} - id \rangle_{Leb},$$

we have

$$\widehat{\mathbf{A}}_o - \widetilde{\mathbf{A}} \xrightarrow{p} 0,$$

which implies

$$\widehat{\mathbf{A}}_o - A \xrightarrow{p} 0.$$

**Theorem 4.4.** *Under the conditions of Theorem 4.3, given the true coefficient  $A$  satisfies Assumption A2, namely,  $A_i \in B_+^1$ ,  $i = 1, \dots, N$ , we have*

$$\widehat{\mathbf{A}} - A \xrightarrow{p} 0.$$

Note that, the convergence rate is lost from Lemma 4.1 to Theorem 4.3 when the empirical Fréchet means are adopted. To maintain the convergence rate, the convergence in Lemma 4.2 need to be moreover uniform, which requires stronger regularity on the random noise functions  $\epsilon_{i,t}$  than currently supposed in Assumption A3. One sufficient assumption is  $\mathbb{E}\{\sup_{x,y} [\epsilon_{i,t}(x) - \epsilon_{i,t}(y)]^2\} \leq L^2(x-y)^2$ ,  $t \in \mathbb{Z}$ ,  $i = 1, \dots, N$ , this will make sure the same regularity holds for the stationary solutions  $\widetilde{\mathbf{F}}_{i,t}$ . A stronger assumption can be  $|\epsilon_{i,t}(x) - \epsilon_{i,t}(y)| \leq L|x-y|$ ,  $\forall x, y \in [0, 1]$ ,  $t \in \mathbb{Z}$ ,  $i = 1, \dots, N$ , almost surely, implying that  $\widetilde{\mathbf{F}}_{i,t}$  is lipschitz almost surely. However such assumptions can be less realistic. Because the asymptotic results do not help the real applications, we do not consider additional assumptions to welcome a large variety of applicable data sets.

## 5 Numerical experiments

In Section 5.1, we firstly demonstrate the consistency result of the proposed estimator using synthetic data. Then, we fit the model on the real data set of age distributions for countries in the European Union in Section 5.2. The estimated coefficient matrix  $\hat{\mathbf{A}}$  allows us to understand the dependency structure of the multivariate distributional time series. In particular, we visualize the learned structure between sensors using a directed weighted graph with the sparse adjacency matrix  $\hat{\mathbf{A}}$ .

### 5.1 Simulations

#### 5.1.1 Generation of the synthetic data

We firstly propose a mechanism to generate valid random distortion functions. To this end, we consider the random functions defined by

$$\epsilon_g = \frac{1 + \xi}{2} g \circ h^{-1} + \frac{1 - \xi}{2} h^{-1}, \quad (5.1)$$

where  $g$  is a non-decreasing right-continuous constant function from  $[0, 1]$  to  $[0, 1]$ ,  $h^{-1}$  is the left continuous inverse of  $h = \frac{1}{2}(g + id)$ , and  $\xi \sim U(-1, 1)$  is a random variable. For any given function  $g$ , we can sample a family of distortion functions  $\epsilon_{i,t} \stackrel{i.i.d.}{\sim} \epsilon_g$ , when sampling  $\xi_{i,t} \stackrel{i.i.d.}{\sim} U(-1, 1)$ . This construction of random distortion functions is inspired by the one proposed in [Zhu and Müller, 2023a, Equation (13)]. However, we have modified their construction of  $h$  and of the random coefficients. It is easy to verify that

$$\mathbb{E}[\epsilon_g] = \frac{1}{2}(g \circ h^{-1} + h^{-1}) = \frac{1}{2}(g + id) \circ h^{-1} = id.$$

To make  $\epsilon_{i,t}$  satisfy additionally Model (3.4) and Assumption A3, we require  $g$  to be furthermore continuous and differentiable. Then on the one hand, since  $g$  is continuous and

non-decreasing, any generated  $\epsilon_g$  is non-decreasing and left-continuous. On the other hand, note that

$$[h^{-1}]' = \frac{1}{h' \circ h^{-1}} = \frac{1}{\frac{1}{2}(g' + 1) \circ h^{-1}} = \frac{2}{g' \circ h^{-1} + 1}.$$

Thus, we have

$$\begin{aligned} \epsilon_{g'} &= \frac{1 + \xi}{2} (g' \circ h^{-1}) \frac{2}{g' \circ h^{-1} + 1} + \frac{1 - \xi}{2} \frac{2}{g' \circ h^{-1} + 1} \\ &= \left( \frac{1 + \xi}{2} g' \circ h^{-1} + \frac{1 - \xi}{2} \right) \frac{2}{g' \circ h^{-1} + 1} \\ &= 1 + \xi - \xi \frac{2}{g' \circ h^{-1} + 1} = 1 + \xi \left( 1 - \frac{2}{g' \circ h^{-1} + 1} \right). \end{aligned}$$

This implies

$$|\epsilon_{g'}| \leq 1 + |\xi| \left| 1 - \frac{2}{g' \circ h^{-1} + 1} \right| \leq 2.$$

The bound comes from  $\xi \sim U(-1, 1)$  and  $g' \geq 0$ , which is hence tight. Thus any  $\epsilon_g$  generated by Formula (5.1) is Lipschitz continuous, with the constant uniformly bounded by 2 over  $\xi$ . Note that Assumption A3 requires the Lipschitz continuity only in expectation. Thus, the i.i.d. samples  $\epsilon_{i,t}$  of any  $\epsilon_g$  satisfy obviously Assumption A3 with the largest  $L = 2$ . Figure 3 shows the function  $g$  used in the simulation and one realization of 30 i.i.d. samples of the resulting  $\epsilon_g$ .

Secondly, we present the procedure to generate the true coefficient matrix  $A$ . We first generate a sparse matrix with the weights all positive in a random way, denoted by  $A^0$ . We then normalize each row of  $A^0$  by the row sum to fulfill Assumptions A2. We denote this last matrix still by  $A^0$ . Based on the previous mechanism for the random distortion function, we take  $L = 2$  in Assumption A4. Lastly, we scale down  $A^0$  by  $(2 + \alpha)\|A^0\|_2$  to obtain a valid  $A$ . We test two values  $\alpha = 0.1$  and  $\alpha = 0.5$  in our experiments.

Given a valid matrix of coefficients  $A$  and samples of  $\epsilon_{i,t}$ , we can then generate the “centered” quantile functions  $\tilde{F}_{i,t}^{-1}$  from Model (3.5). Note that,  $\tilde{F}_{i,t}^{-1}$  are only the simulations of the transformed data. Thus, we have to generate furthermore the population Fréchet

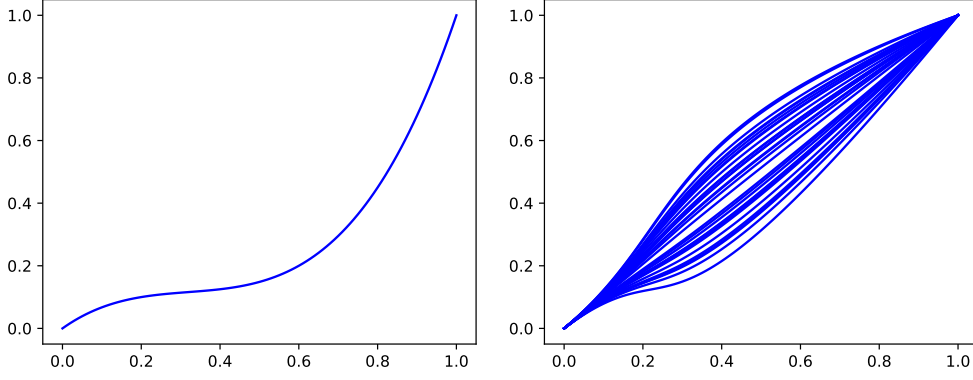


Figure 3: The function  $g$  on the left is given by the natural cubic spline passing through the points  $(0, 0), (0.2, 0.1), (0.6, 0.2), (1, 1)$ . On the right is one realization of 30 i.i.d. samples of the resulting  $\epsilon_g$ .

mean  $F_{i,\oplus}^{-1}$  of each univariate series in order to finally obtain the synthesized “raw” data, as the inverse of transformation (3.2):

$$\mathbf{F}_{i,t}^{-1} = \tilde{\mathbf{F}}_{i,t}^{-1} \oplus F_{i,\oplus}^{-1} := \tilde{\mathbf{F}}_{i,t}^{-1} \circ F_{i,\oplus}^{-1}.$$

We set  $F_{i,\oplus}^{-1}$  as the natural cubic spline of the points:  $(0, 0), (0.2, 0.1), (0.6, 0.2 + 0.2i/N), (1, 1)$ ,  $i = 1, \dots, N$ . The empirical Fréchet mean  $\mathbf{F}_{\hat{\mu}_i}^{-1}$  and the proposed estimator  $\hat{\mathbf{A}}$  are calculated on the synthesized “raw” data  $\mathbf{F}_{i,t}^{-1}$ . In Section 5.1.2, we aim to demonstrate the consistency result given in Theorem 4.4 with the synthetic data.

### 5.1.2 Experiment settings and results

In this experiment, we demonstrate the consistency of the proposed estimator  $\hat{\mathbf{A}}$  for two different values  $N = 10$  and  $N = 100$ . For each  $N$ , we generate two true matrices  $A$  for  $\alpha = 0.1$  and  $0.5$  respectively, according to the procedure presented in Section 5.1.1. With each  $A$ , we calculate the root mean square deviation (RMSD) successively

$$\frac{\|\hat{\mathbf{A}} - A\|_F}{\|A\|_F}, \tag{5.2}$$

with the synthetic data that it generates along time. To furthermore study the mean and the variance of the RMSD (5.2), we run 100 independent simulations for the same  $A$ .

Note that the value of  $\hat{\mathbf{A}}$  we use in Equation (5.2) is the approximation obtained by the projected gradient descent applied to Problem (4.5). Thus the corresponding approximation error also accounts for the deviation which is on the order of the threshold we set in the stopping criteria. For all values of  $N$ , we use the same error threshold. We stop the algorithm as soon as the difference between the previous and the current updates in  $\ell_2$  norm reaches 0.0001, for the resolution of each row  $\hat{\mathbf{A}}_{i:}$ .

We firstly show the evolution of RMSD for  $N = 10, 100$  in Figures 4 and 5, respectively. We can see that, all means and variances of the RMSD decrease towards zero as the sample size  $T$  increases, for each  $N$  and  $\alpha$  value. This demonstrates empirically that, when the model assumptions A2, A3 and A4 hold true for the data, the proposed estimator  $\hat{\mathbf{A}}$  converges to  $A$  in probability, which is implied actually by the convergence of  $\hat{\mathbf{A}}$  to  $A$  in  $L^2$ .

Additionally, we can notice that, the RMSD for  $\alpha = 0.1$  which corresponds to larger  $\ell_2$  norm of  $A$  has a smaller mean in both cases, and also a smaller variance for most of the sample sizes  $T$  investigated.

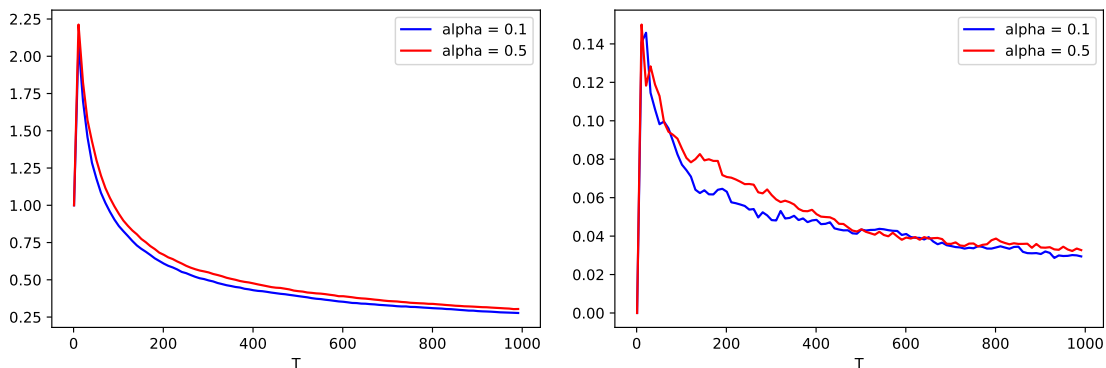


Figure 4: Mean (left) and standard deviation (right) of RMSD for  $N = 10$ . The mean and the variance are calculated over 100 simulations along time  $T$ , every 10 time instants.



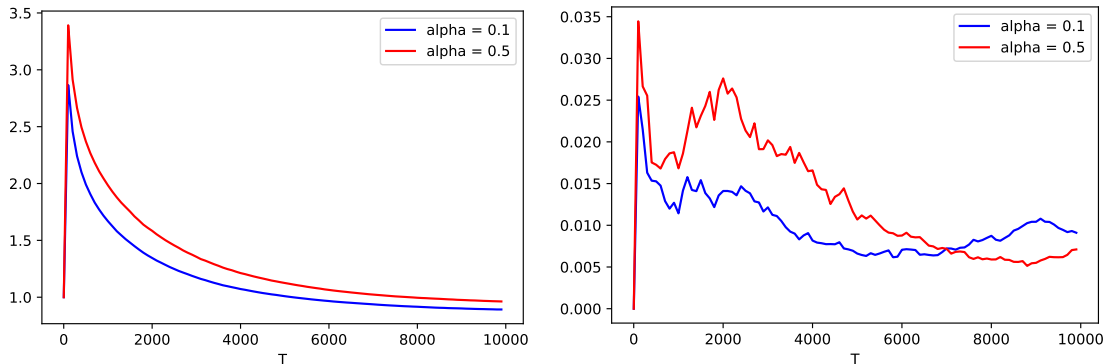


Figure 5: *Mean (left) and standard deviation (right) of RMSD for  $N = 100$ . The mean and the variance are calculated every 100 time instants.*

Also we would like to remark that, during the first few  $T$  values, the samples are insufficient for a meaningful estimation. Thus the projected gradient descent will terminate rapidly, as shown in the very beginning of two subfigures in Figure 6. The output  $\hat{\mathbf{A}}$  will be a zero matrix, since we initialize  $\hat{\mathbf{A}}$  as zero. This results in the low RMSD values during the early phase, since the true  $A$  is generated as a sparse matrix with small weights, as shown in Figures 4 and 5. As  $T$  increases, more entries of  $\hat{\mathbf{A}}$  become non-zero, which brings to the growth of RMSD. Upon the arrival of more new samples,  $\hat{\mathbf{A}}$  starts to converges, meanwhile the RMSD starts to decrease accordingly.

Lastly, we show in Figure 6 the complete execution time of the model fitting on the raw data with respect to the sample size  $T$ . We can see that the execution time increases linearly with respect to  $T$ , and  $A$  with the smaller  $\ell_2$  norm requires slightly less time ( $\alpha = 0.5$ ) than the other. The linear increase comes mainly from the loop over time  $t = 1, \dots, T$  in calculating the empirical Fréchet mean (4.2) and in calculating the matrices  $\hat{\mathbf{\Gamma}}(0), \hat{\mathbf{\Gamma}}(1)$  by their formulas in Equation (4.4). The running time of these calculations is determined by the granularity in the numerical methods to approximate the function composition, function inverse, and the inner product. The granularity applied during this simulation is 0.01, that

is we input/output only the quantile function values at grid  $0, 0.01, \dots, 0.99$  to/from each numerical approximation.

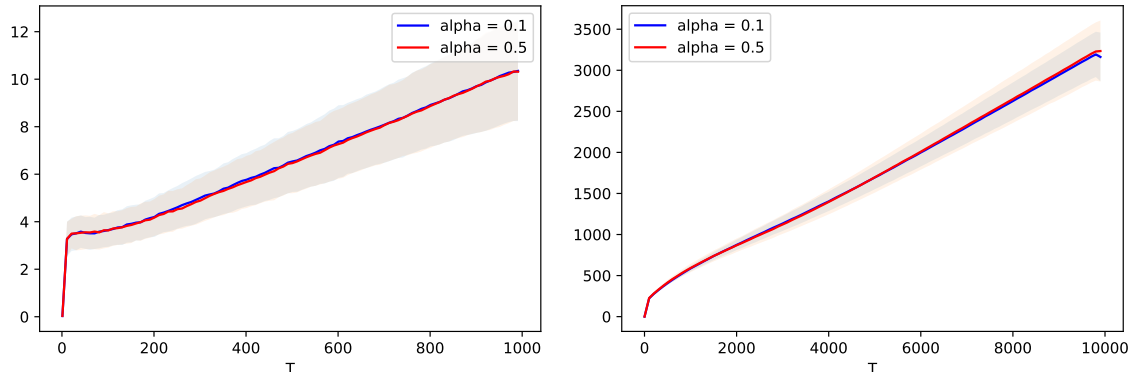


Figure 6: *Calculation time (in seconds) of  $\hat{A}$  with respect to the sample size  $T$  for  $N = 10$  (left) and  $N = 100$  (right). The calculation time counting starts from the computation of the empirical Fréchet means for Data transformation (4.3), and ends when the accelerated projected gradient descent of Problem (4.5) finishes for the last row  $i = N$ .*

## 5.2 Age distribution of countries

We test the proposed model with the real data set illustrated in Figure 1 in the introduction. These data are from the US Census Bureau’s International Data Base<sup>2</sup>, which provides the population estimates and projections for countries and areas by single year of age, over years. We would like to apply the proposed model on this international age distribution data to learn about the links among the changes in the age structures of different countries. Specially, we consider the countries and the micro-states in the European Union and/or Schengen Area. Because the corresponding data used during the model fitting starts in the 1990s, we also include the former European Union member United Kingdom. Note

<sup>2</sup>The data base in open access through <https://www.census.gov/data/developers/data-sets/international-database.html>.

that, Vatican City is not included since it is not available in the data base. Therefore, the list of 34 countries in this study is: Austria, Belgium, Bulgaria, Croatia, Cyprus, Czech Republic, Denmark, Estonia, Finland, France, Germany, Greece, Hungary, Iceland, Ireland, Italy, Latvia, Liechtenstein, Lithuania, Luxembourg, Malta, Monaco, Netherlands, Norway, Poland, Portugal, Romania, San Marino, Slovakia, Slovenia, Spain, Sweden, Switzerland, United Kingdom. Time-wise, we consider the 40 years between 1996 to 2035. 1996 is the earliest year for which the data for all the considered countries is available.

To apply Model (3.4), we firstly represent the distribution of age population, of country  $i$ , at year  $T$ , by  $\mu_t^i$ , with  $T = 1, \dots, 40$  and  $i = 1, \dots, 34$ . Note that the age considered by the data base goes through 0 to 100-plus. Thus we take the 100-plus as 100, and moreover scale down the age by 100 to make the age distribution supported over  $[0, 1]$ . Then we retrieve the quantile function  $F_{i,t}^{-1}$  of  $\mu_t^i$  from the population counts by ages of country  $i$  recorded at year  $T$ , with the numeric methods. In particular, we retrieve the quantile functions using continuous functions which take 0 on  $p = 0$  and 1 on  $p = 1$  so as to be consistent with our assumptions (for details see function `generate_qt_fun` defined in script `age_pop.py` in the code related to this paper).

We fit Model (3.5) on the retrieved functions  $F_{i,t}^{-1}$ ,  $T = 1, \dots, 40$ ,  $i = 1, \dots, 34$ . We use the same stopping criteria as in the simulation, while we apply the granularity of 0.002. The complete execution time of model fitting takes around 78 seconds. Figure 7 shows the inferred coefficient  $A$  visualized as a directed weighted graph, on the geographical map.

Firstly, we can notice that for all countries  $i \in \{1, \dots, 34\}$ , the weight of self-loop  $A_{ii}$  dominates the weights of incoming edges  $A_{ij}$ ,  $j = 1, \dots, 34$ , which are bounded by  $0 \leq \sum_{j=1}^{34} A_{ij} \leq 1$ . This is because the age structure of a country does not change much from one year to another. On the other hand, this also implies the age structure differs

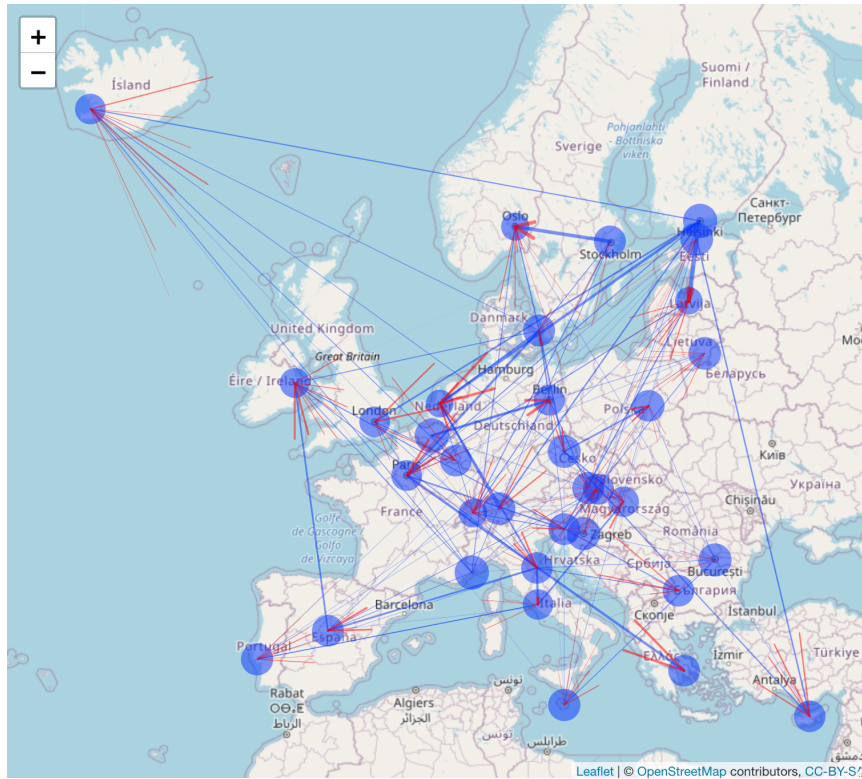


Figure 7: *Inferred age structure graph*. The non-zero coefficients  $A_{ij}$  are represented by the weighted directed edges from node  $j$  to node  $i$ . Thicker arrow corresponds to larger weights. The blue circles around nodes represent the weights of self-loop.

largely across countries. Secondly, the model indicates "significant" cross-country links, in the sense that they are not suppressed to zero by the  $\ell_1$  regularization  $0 \leq \sum_{j=1}^{34} A_{ij} \leq 1$ . The first two largest cross-country weights are respectively: Estonia  $\rightarrow$  Latvia, and Sweden  $\rightarrow$  Norway. To justify the inferred edges, we plot the evolution of age structure of these four countries in Figures 8 and 9.

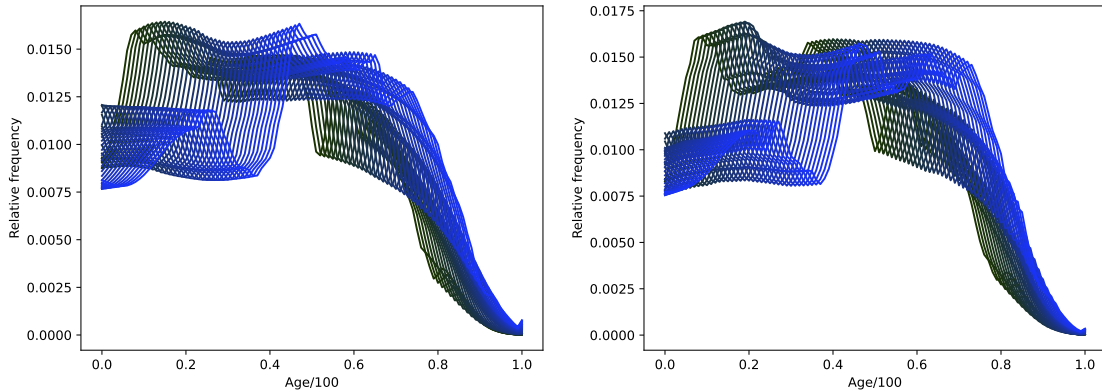


Figure 8: *Evolution of age structure from 1996 to 2036 (projected) of Estonia (left) versus Latvia (right).* Each curve connects the 101 relative frequencies from  $0, 1/100, 2/100, \dots, 1$ , which represents the age structure of a considered year. Lighter curves correspond to more recent years.

We can see that within these four countries, the age structures between the linked countries are similar along time; by contrast, the structures between the unlinked countries are very different. Indeed, these two linked pairs consist both of the countries which share long distances along their borders. Thus, generally, the inferred edges in Figure 7 indicate the similarity of the age structures between countries from 1996 to 2036. Moreover, the directions of the edges imply, at the model level, that, when age structures in the outward countries (for example, Estonia, Sweden) change, it will induce relative changes in the inward countries (respectively, Latvia, Norway). These numeric findings can be furthermore explained in demography or not. On the other, we are interested in the neighbouring

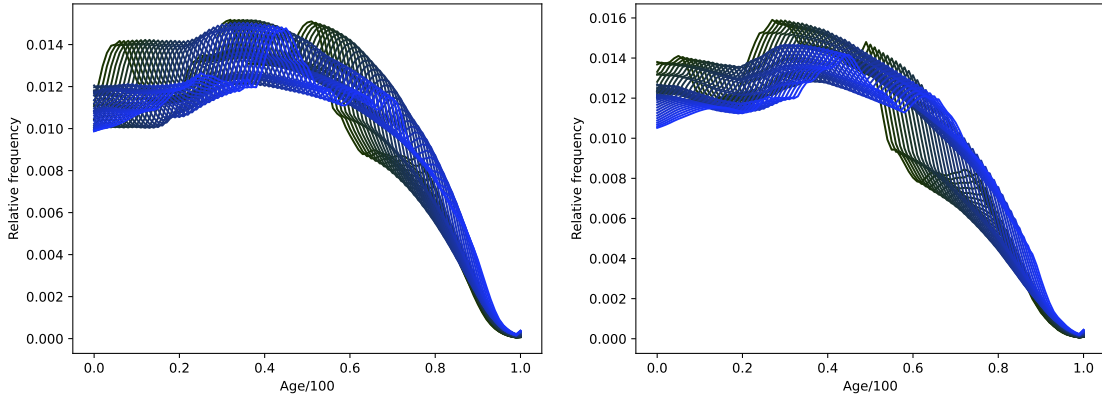


Figure 9: *Evolution of age structure from 1996 to 2036 (projected) of Sweden (left) versus Norway (right).*

countries which are not linked. We verify for example the age structures of France, Italy, in Figure 10. We can see that the age structures are as expected very different.

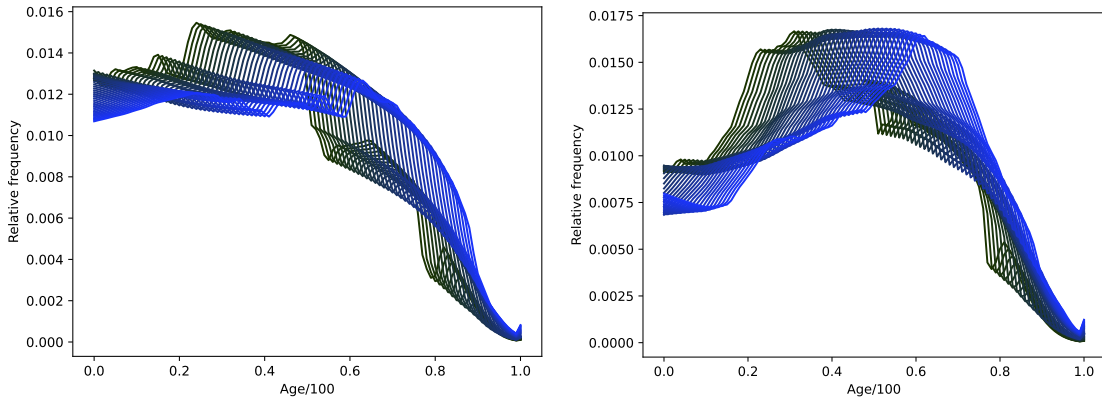


Figure 10: *Evolution of age structure from 1996 to 2036 (projected) of France (left) versus Italy (right).*

Lastly, in Table 1, we provide the first 5 edges of the largest weights. The proposed model reports patterns consistent with the geographical and demographic facts, but is also able to identify new features, which can potentially motivate the follow-up studies in the related domains. These observations show the credibility and usefulness of the proposed model.

Table 1: *Top 5 edges with the largest weights excluding all the self-loops*

	From	To
1	Estonia	Latvia
2	Sweden	Norway
3	Belgium	Germany
4	Finland	Netherlands
5	France	Greece

### 5.3 Bike-sharing network in Paris

To furthermore strength the credibility of the proposed model, we test it on another real data set, which is the bike-sharing data set of Paris from [Jiang et al., 2020]. The data set records the ratio of available bikes of 274 stations, observed over 4417 consecutive hours. We are interested in the temporal evolution of this bike availability of stations, and would like to identify how the stations relate mutually in their evolution using the proposed method. To this end, we firstly represent the data by taking into account the distribution aspect. We introduce the temporal variable  $T$  which represents hours in a day. Accordingly, the distribution  $\boldsymbol{\mu}_t^i$  considered by Model (3.4) represents the distribution of the bike availability of the station  $i$ , at hour  $T$  in a day, with  $T = 1, \dots, 24$  and  $i = 1, \dots, 274$ . Thus the quantile function  $\mathbf{F}_{i,t}^{-1}$  of distribution  $\boldsymbol{\mu}_t^i$  can be retrieved from all the data points of station  $i$  recorded at hour  $T$ , by the numeric methods. We use the similar method as for the age distribution data to retrieve the valid quantile functions, however the implementation is different due to the availability of different quantity types (for details see function `generate_qt_fun` defined in script `bike_net.py` in the code related to this paper).

Note that since these observations are distanced from each other in time, they can

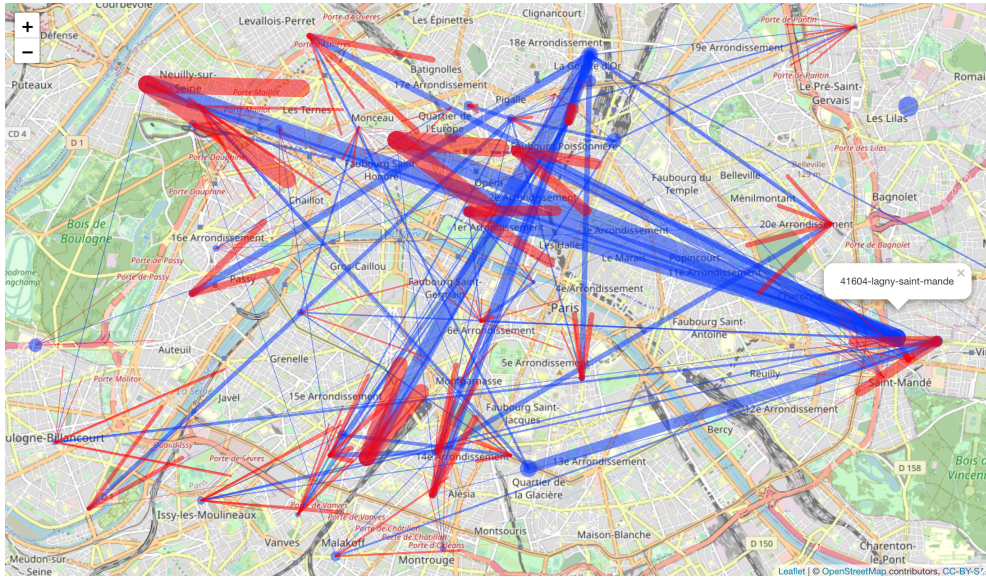


Figure 11: *Subgraph 1 ( 50 nodes chosen randomly )*. For graphical meanings see the caption of Figure 7.

be considered approximately as being independent samples. For more comments on this point, we refer to Remark 5.1. We then fit Model (3.5) on data  $\mathbf{F}_{i,t}^{-1}$ ,  $T = 1, \dots, 24$ ,  $i = 1, \dots, 274$ . We use the same stopping criteria as previously, and we apply the granularity of 0.002. The complete execution time of model fitting takes around 20 minutes. We now demonstrate the visualization of the inferred matrix of coefficients  $A$  on the map of Paris, represented by the directed weighted graph. Since the edges of the complete graph will be densely located in the plot when fitting the graph to the paper size, for better visual effects, we show two subgraphs each of 50 nodes, in Figure 11 and Figure 12 respectively. The complete graph and the subgraphs are available in interactive form at [https://github.com/yiyej/Wasserstein\\_Multivariate\\_Autoregressive\\_Model](https://github.com/yiyej/Wasserstein_Multivariate_Autoregressive_Model).

These figures show some interesting links between the bike utilisation in different areas of Paris. For example, we can notice in Figure 11 that the station *41604-lagny-saint-mande* is much more useful in predicting the stations along the flow from *Saint-Mandé* in southeast



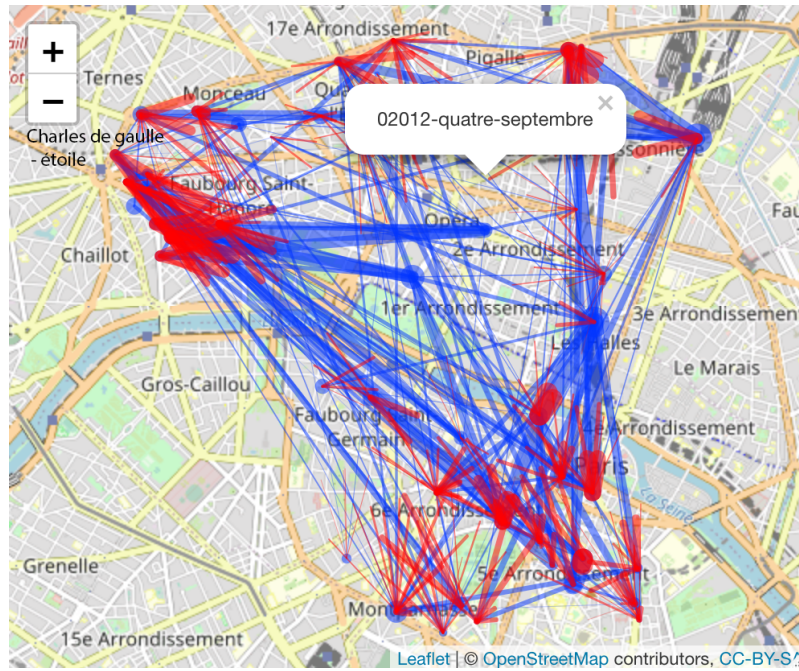


Figure 12: *Subgraph 2 ( the first 50 nodes )*. This subgraph exhibits a more specific area in Paris, isolating the stations numbered 1 to 50.

to *Neuilly-sur-Seine* in northwest. This flow actually goes along the main itinerary of Metro 1 and RER A in Paris, which starts around *Saint-Mandé*. Additionally, we can see in Figure 12 that the stations near *Charles de Gaulle - étoile* (upper left) need to be predicted by numerous stations together, among which is the station *02012-quatre-septembre*. By contrast, station *02012-quatre-septembre* can only be predicted by itself with no edges pointed in. These observations again support the effectiveness of the proposed model and its estimation method.

*Remark 5.1.* Note that another way to represent the data set by distributions is to consider every  $K$  consecutive observations as the i.i.d. samples of a distribution. Thus  $T = 1, 2, \dots, 185/K$  represents the ongoing time in hours. However, the consecutive observations are highly correlated. Moreover, the distribution retrieved in this manner does not clearly represent a random variable. Thus we do not go further with this data representation

method.

## 6 Conclusion

In this paper, we extend the standard VAR models to distributional multivariate AR models, which provides an approach to model a collection of multiple time-dependent probability measures, and to represent their dependency structure by a directed weighted graph at the same time. Especially, the proposed data centering method for random measures allows the development of auto-regressive and regressive models with multiple predictors. Moreover, our empirical study on a real data set demonstrate that, the proposed models equipped with the distributional data representation are the efficient tools for analyzing and understanding the spatial-temporal data. In particular, this paper provides a class of multivariate AR models for distributional time series that favors sparse estimation of auto-regressive coefficients which is beneficial for graph learning.

The authors report there are no competing interests to declare.

## References

- Luigi Ambrosio, Nicola Gigli, and Giuseppe Savaré. *Gradient flows: in metric spaces and in the space of probability measures*. Springer Science & Business Media, 2008.
- Jérémie Bigot, Raúl Gouet, Thierry Klein, and Alfredo López. Geodesic PCA in the wasserstein space by convex PCA. *Annales de l'Institut Henri Poincaré, Probabilités et Statistiques*, 53(1):1–26, 2017.
- Sergey Bobkov and Michel Ledoux. One-dimensional empirical measures, order statistics and kantorovich transport distances. *preprint*, 7127347, 2014.

- Denis Bosq. *Linear processes in function spaces: theory and applications*, volume 149. Springer Science & Business Media, 2000.
- Elsa Cazelles, Vivien Seguy, Jérémie Bigot, Marco Cuturi, and Nicolas Papadakis. Log-PCA versus geodesic PCA of histograms in the wasserstein space. *arXiv preprint arXiv:1708.08143*, 2017.
- Yaqing Chen, Zhenhua Lin, and Hans-Georg Müller. Wasserstein regression. *Journal of the American Statistical Association*, pages 1–14, 2021.
- Zhicheng Chen, Yuequan Bao, Hui Li, and Billie F Spencer Jr. LQD-RKHS-based distribution-to-distribution regression methodology for restoring the probability distributions of missing shm data. *Mechanical Systems and Signal Processing*, 121:655–674, 2019.
- Laya Ghodrati and Victor M Panaretos. Distribution-on-distribution regression via optimal transport maps. *Biometrika*, 109(4):957–974, 2022a.
- Laya Ghodrati and Victor M Panaretos. Distribution-on-distribution regression via optimal transport maps. *Biometrika*, 01 2022b. asac005.
- Lütkepohl Helmut. *New introduction to multiple time series analysis*. Springer Berlin Heidelberg, 2005.
- Yiye Jiang, Jérémie Bigot, and Sofian Maabout. Sensor selection on graphs via data-driven node sub-sampling in network time series. *arXiv preprint arXiv:2004.11815*, 2020.
- Piotr Kokoszka, Hong Miao, Alexander Petersen, and Han Lin Shang. Forecasting of density functions with an application to cross-sectional and intraday returns. *International Journal of Forecasting*, 35(4):1304–1317, 2019.

- Stefano Mazzucco and Bruno Scarpa. Fitting age-specific fertility rates by a flexible generalized skew normal probability density function. *Journal of the Royal Statistical Society: Series A (Statistics in Society)*, 178(1):187–203, 2015.
- Victor M Panaretos and Yoav Zemel. *An invitation to statistics in Wasserstein space*. Springer Nature, 2020.
- Neal Parikh and Stephen Boyd. Proximal algorithms. *Foundations and Trends in optimization*, 1(3):127–239, 2014.
- Alexander Petersen and Hans-Georg Müller. Functional data analysis for density functions by transformation to a hilbert space. *The Annals of Statistics*, 44(1):183–218, 2016.
- Alexander Petersen and Hans-Georg Müller. Fréchet regression for random objects with euclidean predictors. *The Annals of Statistics*, 47(2):691–719, 2019a.
- Alexander Petersen and Hans-Georg Müller. Wasserstein covariance for multiple random densities. *Biometrika*, 106(2):339–351, 2019b.
- Han Lin Shang and Steven Haberman. Forecasting age distribution of death counts: An application to annuity pricing. *Annals of Actuarial Science*, 14(1):150–169, 2020.
- Jerome Thai, Cathy Wu, Alexey Pozdnukhov, and Alexandre Bayen. Projected sub-gradient with  $\ell_1$  or simplex constraints via isotonic regression. In *2015 54th IEEE Conference on Decision and Control (CDC)*, pages 2031–2036. IEEE, 2015.
- Cédric Villani. *Topics in optimal transportation*, volume 58. American Mathematical Soc., 2021.
- Wei Biao Wu and Xiaofeng Shao. Limit theorems for iterated random functions. *Journal of Applied Probability*, 41(2):425–436, 2004.

Chao Zhang, Piotr Kokoszka, and Alexander Petersen. Wasserstein autoregressive models for density time series. *Journal of Time Series Analysis*, 2021.

Changbo Zhu and Hans-Georg Müller. Autoregressive optimal transport models. *Journal of the Royal Statistical Society Series B: Statistical Methodology*, 85(3):1012–1033, 2023a.

Changbo Zhu and Hans-Georg Müller. Geodesic optimal transport regression. *arXiv preprint arXiv:2312.15376*, 2023b.